Spherical-Harmonic Distribution Analysis of Coronae in Relation to Volcanic Features on Venus

Wesley S. Tucker[1] and Andrew J. Dombard[1]

[1]Department of Earth and Environmental Sciences, University of Illinois Chicago, Chicago, IL.

Corresponding author: Wesley Tucker (wtucke5@uic.edu)

Key Points:

- A new subset of coronae shows topographic changes post-lava flow emplacement.
- Spectral analysis reveals strong long-wavelength similarities between coronae and large volcanoes.
- Volcanism plays a crucial role in corona formation and should be considered central in future models of formation.

Abstract

Venus boasts an abundance of volcano and volcano-like structures. Synthetic aperture radar images of the surface have revealed extensive evidence of volcanism, including lava flows and edifices. Volcanic activity is further supported by crater statistics, and analysis of topography and gravity data. Unique to Venus, coronae are quasi-circular, volcano-tectonic features exhibiting diverse volcanic characteristics. Despite this, volcanism is often under-represented in formation models. We identify a new subset of coronae that display topographic change subsequent to the emplacement of lava flows within their fracture annuli, pointing to the critical role of volcanism in the formation of these coronae. Through spherical-harmonic distribution analysis, we find that this new subset is spatially related to the full coronae database, pointing to an intrinsic process of coronae formation. Furthermore, coronae exhibit strong correlations and similar spectral shapes at low spherical harmonic degrees with large volcanoes, suggesting a shared geodynamic origin. Our findings underscore the pivotal role of volcanism in coronae formation and highlight the need for future research that integrates magmatic processes into geophysical models.

Plain Language Summary

Venus's surface has a large number of volcanoes and features with characteristics similar to volcanoes. Radar imagery of the surface reveals signs of volcanism such as lava flows and volcanically built mountains. A unique volcanic feature, found only on Venus, are coronae, which have circular fractures and various types of associated volcanic activity. Explanations of how coronae form often do not consider the role of volcanic activity. In our study, we identify a new group of coronae that have undergone changes in topography after lava erupted and flowed over them, which has been interpreted as volcanism having a central role in corona formation. The locations of this subset of coronae on the surface fits well with all other coronae, suggesting the processes that caused this topographic change occur throughout the corona population and are a basic part of how all coronae form. Additionally, we find that coronae have a similar pattern on the surface to large volcanoes, which indicates a shared, volcanically based origin. Our work shows that in order to better understand coronae, we need to consider the role of volcanism in their formation.

1 Introduction

NASA's Magellan spacecraft, with its single radar system, provided data covering nearly the entire surface of Venus. The high-resolution (~75 m/pix) synthetic aperture radar (SAR) data presented a detailed view of the surface, enabling the identification of extensive volcanic features beyond the capabilities of the preceding Venera 15/16 missions. These improved data revealed a more extensive range of volcanoes, with diameters from less than 1 km to over 100 km (e.g., Guest et al., 1992; Head et al., 1992), and provided a more detailed view of the intriguing volcano-tectonic structures known as coronae (e.g., Squyres et al., 1992; Stofan et al., 1992). Many hypotheses have been proposed regarding the formation and evolution of coronae, and the debate has continued since the early days of the Magellan mission (e.g., Copp et al., 1998;

Davaille et al., 2017; DeLaughter & Jurdy, 1999; Dombard et al., 2007; Gerya, 2014; Gülcher et al., 2021; Hoogenboom & Houseman; 2006; Janes & Squyres, 1995; Koch & Manga; 1996; Lang and López, 2015; Smrekar & Stofan, 1997).

Numerous volcanoes and volcano-like structures are scattered across the surface of Venus. Using Venera 15/16 data, volcanoes were initially binned into three size classes: small, intermediate, and large (e.g., Slyuta, 1990; Slyuta & Kreslavsky, 1990). Following NASA's Magellan mission, this classification system continued, in part for consistency (e.g., Head et al., 1992), but also for convenience as the individual SAR swaths were roughly 20 km wide during the early stages of the mission (Crumpler et al., 1997). Further, these divisions were consistent with the cumulative size distribution of the 1195 volcanoes identified by Crumpler et al. (1997). Roughly half of the edifices identified in that study had diameters between 20 km and 100 km.

A recent survey substantially expanded on the number of volcanoes. Hahn & Byrne (2023) identified ~85,000 edifices. To skirt away from the arbitrariness of early size binning, the authors employed "mixture modeling" to determine if there are discrete populations of volcanoes based on their diameters and found two distinct exponential distributions when splitting the data into two sets: volcanoes between 5 km and 63 km (diameters were not measured for volcanoes $\leq$ 5 km) and volcanoes > 63 km (see Figure 6 of Hahn & Byrne, 2023).

A specific focus of Venusian volcano studies has been on shield volcanoes, which make up a significant percentage of the observed edifices. Early observations from Venera 15/16 data noted the high number of small shield volcanoes, ~22,000, with just 25% of the surface being imaged at the time (Aubele & Slyuta, 1990). Shield volcanoes often occur in relatively high spatial concentrations, termed "shield fields" or "volcanic fields" (Figure 1). The most recent catalogue of volcanoes included 566 volcanic fields (Hahn & Byrne, 2023). Shield volcanoes display small topographic signatures and diameters of 20 km or less. They are proposed to result from distinct crustal melt sources that are unable to supply magma at rates sufficient for building a single edifice (Guest et al., 1991; Head et al., 1992; Ivanov et al., 2017; Thomas & Lang, 2016).

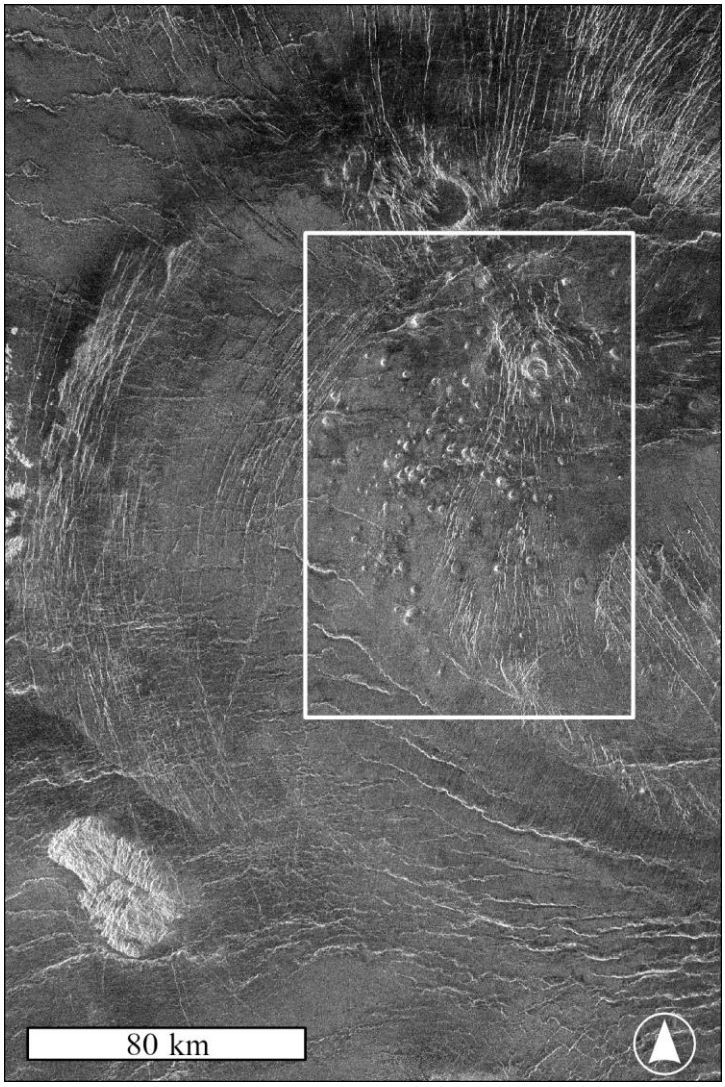

Figure 1. Magellan SAR image (75 m/pix) of a cluster of shield volcanoes (white box) from a volcanic field identified by Hahn & Byrne (2023) within Belet-ili Corona (6°N, 20°E). Circular, radar bright spots represent individual shield volcanoes.

Venus hosts more than 500 coronae, quasi-circular volcano-tectonic features (Stofan et al., 2001a). Being unique to Venus, their existence might provide critical insights into the differences between Earth's and Venus's lithospheres. For instance, they may contribute significantly to the heat loss budget on Venus, which is difficult to explain due to the lack of plate tectonics (e.g., Smrekar & Stofan, 1997; Smrekar et al., 2018).

The term “corona” refers to the features’ morphology, specifically their circular structure composed of concentric fracture and ridge annuli (Barsukov et al., 1986). A survey of Magellan SAR images by Stofan et al. (2001a) significantly expanded the corona database to roughly its current size (see section 2.1). Though initially classified based solely on morphologic characteristics, a more comprehensive understanding of coronae emerges from four critical observations: an annulus of tectonic structures, varied and complex topography, a wide range of diameters, and associated volcanism (e.g., Dombard et al., 2007; Tucker & Dombard, 2023a).

The critical observations underscore the diverse characteristics exhibited by coronae. For example, the size of the fracture annulus within coronae varies from 10 km to over 150 km (Stofan et al., 1992). Furthermore, the topographic signatures of coronae are diverse and complex. Despite this, they have been categorized into nine distinct classifications (Smrekar & Stofan, 1997; Stofan et al., 1997, 2001). Coronae cover a wide range of diameters, ranging from as small as 60 km to as large as 2600 km for Artemis Corona. However, Artemis Corona is approximately 1600 km wider than the next largest corona, Heng-O, and it may have formed through a completely different set of processes (e.g., Davaille et al., 2017; Hansen, 2002; McKenzie et al., 1992; Sandwell & Schubert, 1992).

Last, coronae are closely associated with various forms and intensities of volcanism. Large lava flow fields, of the order of terrestrial flood basalts, have been linked to sources associated with coronae (e.g., Roberts & Head, 1993). Individual lava flows are also observable within and radiating from the fracture annuli (e.g., Tucker & Dombard, 2023a). Additionally, other volcanic edifices, such as tholi or small shield volcanoes, are often found within or on corona annuli (e.g., Lang & López, 2015; Roberts & Head, 1993; Russell & Johnson, 2021; and cf. Fig. 1).

Venus has a relative lack of impact craters when compared to other bodies in the solar system, apart from Earth, indicating a youthful surface and a history of resurfacing. This finding, coupled with the presence of abundant volcanic features, raises questions regarding the current level of geologic activity on Venus. Surveys of the crater population have identified approximately 900 impact structures (e.g., Herrick et al., 1997; Phillips et al., 1992; Schaber et al., 1992) with a spatial distribution that cannot be distinguished from a random population (e.g., Hauck et al., 1998; Phillips et al., 1992; Strom et al., 1994). The seemingly random distribution

of craters (see Figure 2 of Herrick et al., 2023) has led to an inferred global surface age ranging from approximately 300 to 800 Myr (e.g., Hauck et al., 1998; McKinnon et al., 1997). Venus does not show major effects of erosion (Arvidson et al., 1992), and thus the only explanation for the lack of cratering is either volcanism or tectonism (Hauck et al., 1998). Two hypotheses have emerged to explain Venus's cratering: a catastrophic resurfacing model (Schaber et al., 1992; Strom et al., 1994) or a continuous (or equilibrium) resurfacing model (Phillips et al., 1992), although, the catastrophic resurfacing model is no longer thought to be valid (e.g., Guest & Stofan, 1999; Hauck et al., 1998; Herrick & Sharpton, 2000). On this basis, Venus could be volcanically active today.

Indeed, several studies have presented intriguing findings of potential recent volcanism. For instance, thermal emission data from the Visible and Infrared Thermal Imaging Spectrometer (VIRTIS) on the European Space Agency's Venus Express spacecraft revealed emissivity anomalies in lava flows in the Themis, Imdr, and Dione Regiones, all of which are suspected areas of hotspot volcanism. The absence of surface weathering in these regions suggests that these lava flows could be as young as 250,000 years (Smrekar et al., 2010). Most recently, Herrick and Stanley (2023) observed a change in vent geometry of a shield volcano between two Magellan image cycles. The first image was interpreted as a drained volcanic vent, which appeared to refill and form a lava lake by the time of the subsequent imaging cycle.

Studies of gravity and topography data have also provided insights into the activity states of volcanoes and coronae on Venus. The occurrence of uncompensated geoid highs in Atla, Beta, and Eistla Regiones have been interpreted as areas underlain by active mantle plumes (e.g., Anderson & Smrekar, 2006; Grimm & Phillips, 1992; Smrekar, 1994; Stofan et al., 1995). Johnson and Richards (2003) identified coronae as candidates for potential current activity based on their compensated state. Dombard et al. (2007) further examined the gravity and topography of coronae in the BAT region, concluding that some of these features are likely currently underlain by an impinged thermal due to positive topography and geoid anomalies coinciding with negative Bouguer anomalies.

A connection between the topographic signatures of coronae and their activity states has also been proposed (e.g., Smrekar & Stofan, 1997). Gülcher et al. (2020) compared the topographic signatures generated by their three-dimensional thermomechanical simulations to

the topography of existing coronae. They concluded that 37 coronae were likely active as their topography matched the model's plume-lithosphere interaction stages. However, these methods primarily assume that mantle upwelling and subsurface solid-state flow influence corona morphology and formation. In contrast, other volcanic-related processes, such as magmatic loading (e.g., Dombard et al., 2007), collapsing magma reservoirs (e.g., Lang & López, 2015), or volcanic construction (e.g., McGovern et al., 2013), could be responsible for coronae formation.

It is well established that both coronae and volcanoes show spatial clustering in the BAT region (e.g., Hahn & Byrne, 2023; Head et al., 1992; Squyres et al., 1993; Stofan et al., 1992, 1995) (Figure 2). Their distribution, along with their relationship to topography and gravity, may provide insights into mantle flow dynamics, and formation mechanisms.

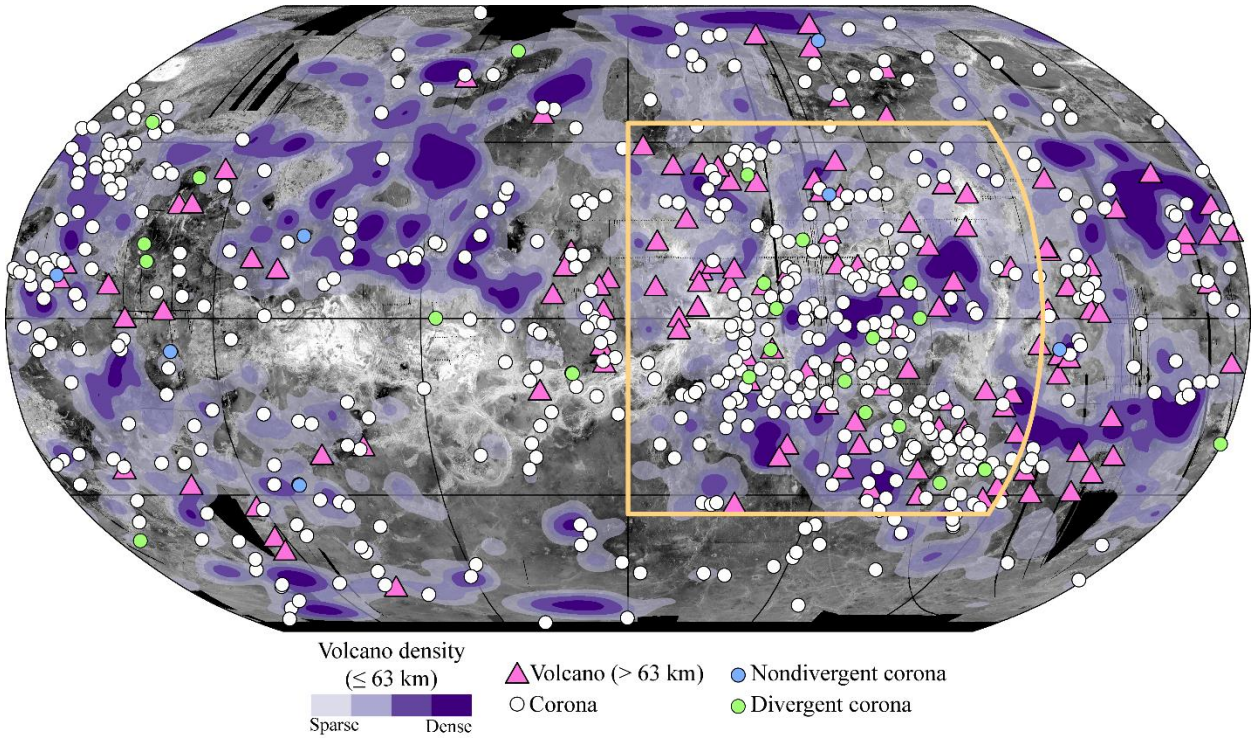

Figure 2. Global distribution of volcanoes and corona subsets on Venus. Volcanoes with diameters less than 63 km (N=84,894) are displayed using a kernel density estimate with a 500 km search radius (Silverman, 1986). The map is centered on 180° in Robinson projection with a thrice compressed (~2025 m/pixel) Magellan SAR image (C3-MIDR) base layer. The yellow outline is the Beta-Atla-Themis (BAT) region. For dataset descriptions, see section 2.

In this study, we explore the volcanic nature of coronae in greater detail. We identify a new subset of coronae that have undergone topographic changes within the fracture annuli since the emplacement of lava flows. This phenomenon, previously described by Tucker and Dombard (2023a) in detail at Atete and Aruru Coronae, suggests a magmatic influence on corona topography. To extend our understanding, we employ spatial analysis techniques and spherical harmonics to investigate the global distribution and characteristics of volcanoes, coronae, and subsets of these data. We focus on the interplay between coronae and volcanoes, with a specific emphasis on the role of volcanic processes in the formation of coronae. Through our findings, we aim to underscore the significance of coronae in our understanding of the volcanic processes shaping Venus's surface and to reiterate the inherently volcanic nature of coronae.

2 Data and Methods

In our spherical harmonic analysis, we utilize a diverse selection of datasets. These include comprehensive catalogues of both volcanoes and coronae. In addition, we analyze specific subsets from these catalogues that have been compiled by previous studies. We also analyze a novel subset of coronae, identified for this work, characterized by lava flows within the fracture annuli that diverge from the modern downhill direction. In addition to the datasets discussed below, we use spherical harmonic coefficients from models of topography (VenusTopo719) (Wieczorek, 2015) and gravity (MGNP180U) (Konopliv et al., 1999).

2.1 Compiled datasets

A contemporary survey of volcanoes on Venus identified 85,021 volcanic features (Hahn & Byrne, 2023). The authors catalogued volcanoes into three diameter bins: < 5 km (small), 5 to 100 km (intermediate), and >100 km (large). Of these, the majority (99%) were less than 5 km in diameter, while 729 were intermediate sized, and 118 were larger than 100 km. Moreover, Hahn and Byrne (2023) identified 566 clusters of shield volcanoes, which they termed volcanic fields, containing shield volcanoes with diameters of 20 km or less. Hahn and Byrne (2023) defined the volcano size bins to aid in the mapping and measuring of edifices. Volcanoes ≤ 5 km were marked as point features, while the extents of volcanoes > 5 km were digitized, and their diameters were calculated. However, for their spatial analysis (see Figure 7 of Hahn & Byrne, 2023), the authors classified volcanoes into those ≤ 63 km and those > 63 km (see section 1). To be consistent with this modern catalogue of volcanoes, we will utilize these two size bins for our

subsets of the volcano catalogue. Notably with a minimum corona diameter of ~60 km, all coronae are in the size range of large volcanoes.

We analyze coronae on the surface of Venus by combining the Type 1 and Type 2 corona dataset from Stofan et al. (2001a) and the Venus nomenclature database from the USGS (planetarynames.wr.usgs.gov). To further refine our analysis, we incorporate a subset of the combined corona database of coronae with lava flows that diverge from the downslope direction.

2.2 Corona associated divergent lava flows

Building on our preliminary work on Aruru and Atete Coronae and using the same methodology (Tucker & Dombard, 2023a), we have identified coronae with lava flows within their fracture annuli that diverge from the modern downhill slope direction in the combined corona dataset. Full resolution (~75 m/pix) Magellan synthetic aperture radar (SAR) images are imported into ESRI ArcMap and stretched to enable the identification of discrete lobate and digitate flow features. At coronae with suitable flow features, flow centerlines are mapped, and the azimuthal orientation is determined using the start and end points.

To determine if the lava flows follow the modern topography, the line azimuth is compared to the regional slope facing direction (i.e., aspect). A 25 km buffer is placed around the center point of each flow line, and the mean regional aspect is determined for the buffer area. Aspect rasters are derived from Magellan global topographic data records (GTDR), and where available, stereo-derived digital elevation models from Herrick (2020). Comparing the flow line azimuth to the regional aspect provides data on changes in topography since the flows were emplaced. Two new subsets of corona are recorded: coronae with intra-annular divergent flows and coronae without intra-annular divergent flows. If the number of mapped flows that diverge from the downhill direction is twice the number of mapped flows that do not have flow divergence, we consider that corona as one with divergent flows. To determine the appropriate cutoff for classifying coronae based on divergent and nondivergent lava flows, we analyze coronae exhibiting both flow types (i.e., ignoring coronae with only divergent lava flows). A predominant cluster is present around a ratio of 1, indicating a near-equivalent presence of both flow types. Additionally, a Kernel Density Estimate (KDE) analysis produces a pronounced peak near this ratio, with the density decreasing for higher ratios. Therefore, we consider a cutoff at a

ratio of 2 to be statistically and contextually apt for distinguishing between coronae with both flow types and those where divergent flows prevail.

A total of 72 coronae, a clear subset of the total coronae population, had visible flows in their interiors; however, 42 of those had either too few flow units or flows without discernable margins. Divergent flows were identified in 24 corona interiors, while 6 did not have divergent lava flows (Figure 2) (Supporting Information Table S1). For simplicity, we will refer to a corona as either divergent or nondivergent when referring to coronae with lava flows that either diverge or do not diverge from the modern downhill direction.

2.3 Spherical harmonic analysis

To examine the distribution of coronae that have undergone topographic change, we use spectral analysis. Based on spherical harmonics, information about the wavelength that best describes the distribution can be discerned via power spectra. Spherical harmonic analysis is a useful tool for assessing the correlations and anticorrelations of global data subsets. Using this method will allow for comparison of the full corona dataset with the global volcano database and subsets of the corona database described above. Further, spectra of these data will be compared to long-wavelength features represented by continuous data such as gravity and topography.

The fully normalized spherical harmonic expansions of the distribution are given by (Johnson & Richards, 2003; Kirchoff et al., 2011)

$$f_{lm}(\theta,\phi) = P_l^m(\cos\theta)(c_{lm}\cos m\phi + s_{lm}\sin m\theta), \quad (1)$$

where ϕ is the longitude, θ is the colatitude, and P_l^m is the associated Legendre polynomial of degree l and order m. The cosine and sine coefficients, c_{lm} and s_{lm}, are determined by projecting the locations of the features in the dataset onto a particular spherical harmonic:

$$c_{lm} = \sqrt{\frac{(2-\delta_{0m})(2l+1)(l-m)!}{4\pi(l+m)!}}\sum_{n=1}^{N} P_l^m(\cos\theta_n)\cos m\phi_n \quad (2a)$$

$$s_{lm} = \sqrt{\frac{(2-\delta_{0m})(2l+1)(l-m)!}{4\pi(l+m)!}}\sum_{n=1}^{N} P_l^m(\cos\theta_n)\sin m\phi_n, \quad (2b)$$

where N is the total number of features (coronae or volcanoes) in the dataset; in this definition, the spherical harmonics are fully normalized. The Kronecker delta function, δ_{lm}, is

$$\delta_{0m} = \begin{cases} 1, & m = 0, \\ 0, & m \neq 0. \end{cases} \quad (3)$$

We use a maximum degree l = 20 for the expansion, which follows previous spherical harmonic analysis on Venus (e.g., Johnson & Richards, 2003). Figure 3 illustrates the relationship between spherical harmonic coefficients and the location of the features at several spherical harmonic degrees.

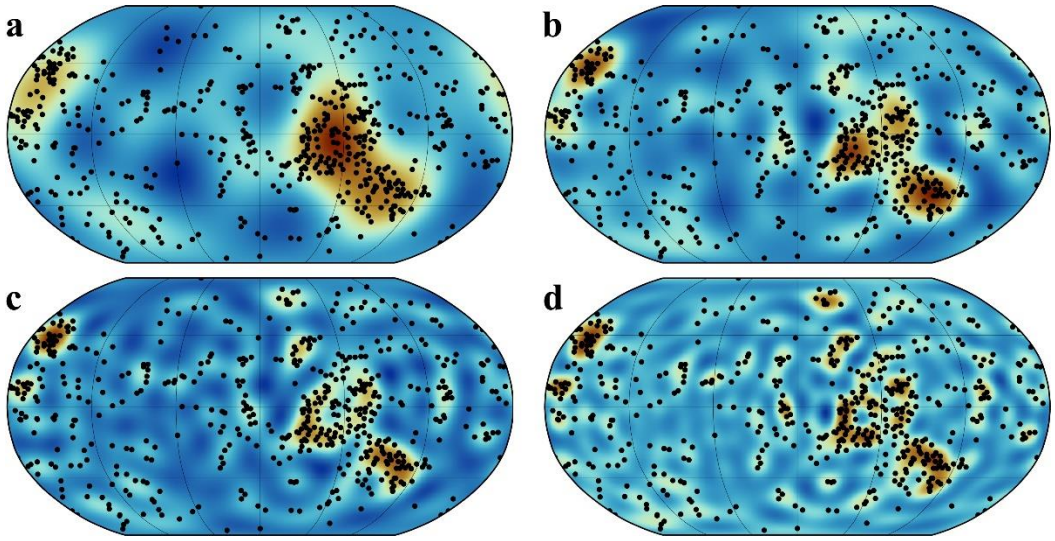

Figure 3. Robinson projected maps showing spherical harmonic representations of the full coronae database truncated at (a) l = 5, (b) l = 10, (c) l = 15, and (d) l = 20. Black dots are locations of coronae from the combined corona database. Hot colors (red) indicate relatively more dense concentrations of coronae and cool colors (blue) are less dense. All maps are centered at 180°E.

The spectral power is normalized for the number of features in a distribution, and with this normalization, will appear white for random distributions (Ribe de Valpine, 1994; Richards et al., 1988; Kirchoff et al., 2011):

$$S_l = \frac{4\pi}{N(2l+1)} \sum_{m=o}^{l} (c_{lm}^2 + s_{lm}^2). \quad (4)$$

Additionally, we check for randomness of the features by comparing their spectra to randomly generated latitude and longitude points on a sphere. Over 10,000 iterations, random latitude-longitude points are generated for the number of samples in the dataset of interest. In

each iteration, the latitudes and longitudes of points are randomly generated following a uniform distribution on a sphere. The transformation functions $\theta = 2\pi u$ and $\phi = \cos^{-1}(2v - 1)$ where u and v are random variates, are utilized for this purpose. To prevent the random points from being artificially close to each other (e.g., if two coronae have diameters of 50 km each their centers must be >100 km from each other), the ranges of the radii of the randomly generated points are chosen to align with the distribution of the radii in the dataset. Each random point is assigned a radius value dictated by the probability distribution that best represents the size distribution of the dataset to which the random distributions is compared (e.g., a lognormal of the corona diameters). The 1st to 99th percentile of the power per degree of the 10,000 iterations are extracted, effectively creating a 98% confidence envelope and ignoring potential outliers. Spectra with power that falls within the envelope indicates that there would be a less than 1 in 10,000 chance that they can be distinguished from the spectra of a random population.

Comparison of power spectra between two datasets, or between the full population and a subset of that population, is performed by obtaining the correlation coefficient per degree, r_l, of two distributions with (Johnson & Richards, 2003; Kirchoff et al., 2011; Richards et al., 1988)

$$r_l = \frac{\sum_{m=0}^{l}(c_{lm}g_{lm} + s_{lm}h_{lm})}{\sqrt{\sum_{m=0}^{l}(c_{lm}^2 + s_{lm}^2)\sum_{m=0}^{l}(g_{lm}^2 + h_{lm}^2)}}. \quad (5)$$

Correlation values range from -1 to 1. Perfectly positive correlated distributions have a value of 1, anticorrelations are represented by a value of -1, and distributions with no correlation have a value of 0. Further, we use a two-tailed Student-t distribution to calculate the confidence interval for a percentage t_α, with degrees of freedom 2l for the correlation coefficients (Press et al., 1987; Wetherill, 1982)

$$r_l = \pm t_\alpha \sqrt{\frac{1}{2l + t_\alpha^2}}. \quad (6)$$

Datasets with distributions that are similarly represented by a spherical harmonic degree will be strongly correlated at that degree. As discussed by Kirchoff et al. (2011), the lack of direct superposition of features does not mean that the features will be anti-correlated, and the position of neighboring features affects correlation coefficients at high degrees. Similarly, equations (3a) and (3b) ensure that strong correlation will occur at low degrees for similar distributions.

3 Results

The locations of volcanoes, coronae, and their subsets are shown in Figure 2, offering a qualitative view of their distribution. To quantify these distributions and understand their relationships across varying spatial scales, we turn to the analysis of their power spectra. This method allows for the exploration of the spatial distribution characteristics of these features and their subsets, thereby offering insights into their potential correlations and similarities.

The spectra for divergent, nondivergent, and the full population of coronae is shown in Figure 4a. We have normalized the spectra to equal 1 at l =2 for easy comparison. The nondivergent coronae spectrum is white across all wavelengths, a pattern likely influenced by the small sample size (N=6). In contrast, the spectra for the full population and the divergent subset exhibit similarity at low spherical harmonic degrees, transitioning from a red (decreasing power with wavelength to a white (flat) spectrum at higher degrees. This shift suggests a move towards a more random or evenly distributed pattern at smaller scales. When examining the correlation at low spherical harmonic degrees, we observe a strong relationship between the full corona population and the divergent subset, indicating a shared large-scale spatial pattern (Figure 4b). However, this correlation weakens at short wavelengths, staying below the 80% confidence level for l >14.

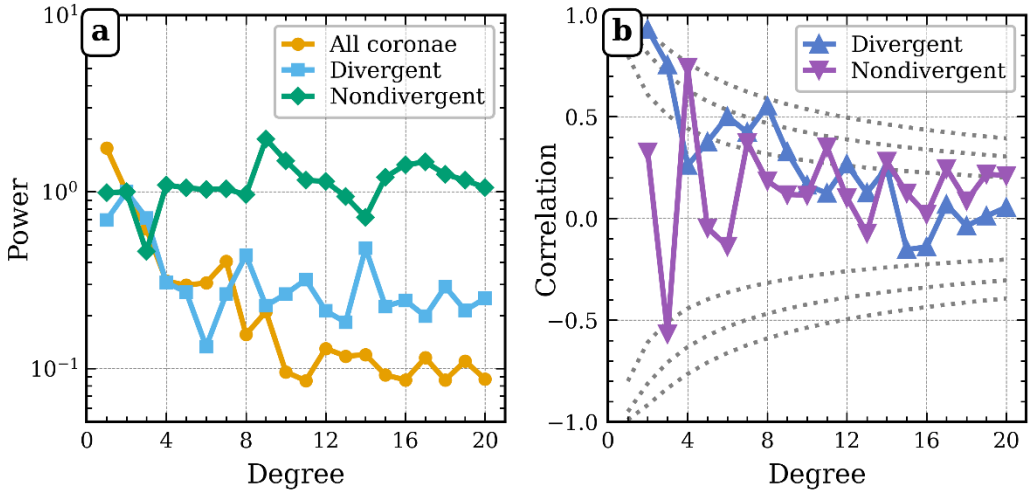

Figure 4. (a) Spectra for the full catalogue and subsets of coronae normalized to equal 1 at l =2. (b) Correlation per degree between all coronae and divergent and nondivergent coronae. Dotted lines represent 80%, 95% and 99% confidence intervals, indicating a 20%, 5%, and 1% chance of randomness in correlation coefficients for points outside these lines, respectively.

Figure 5a shows the normalized power spectra of the full catalogues of coronae and volcanoes, topography, and geoid. The geoid and topography spectra are red across all wavelengths and well correlated visually, consistent with previous studies (e.g., Johnson & Richards, 2003; Konopliv et al., 1999; Rappaport et al., 1999; Wieczorek, 2015). Both the full datasets of volcanoes and coronae exhibit similar spectral shapes at long wavelengths (l < 10), transitioning from red to relatively white spectra at higher degrees. However, the volcano spectrum's absolute power is approximately two orders of magnitude greater than that of the coronae across all wavelengths. Furthermore, the volcano spectrum lies outside of the 99% confidence bounds of the 10,000 random distributions (Figure 5c). Both outcomes are likely the product of the large number of volcanoes providing good statistical robustness.

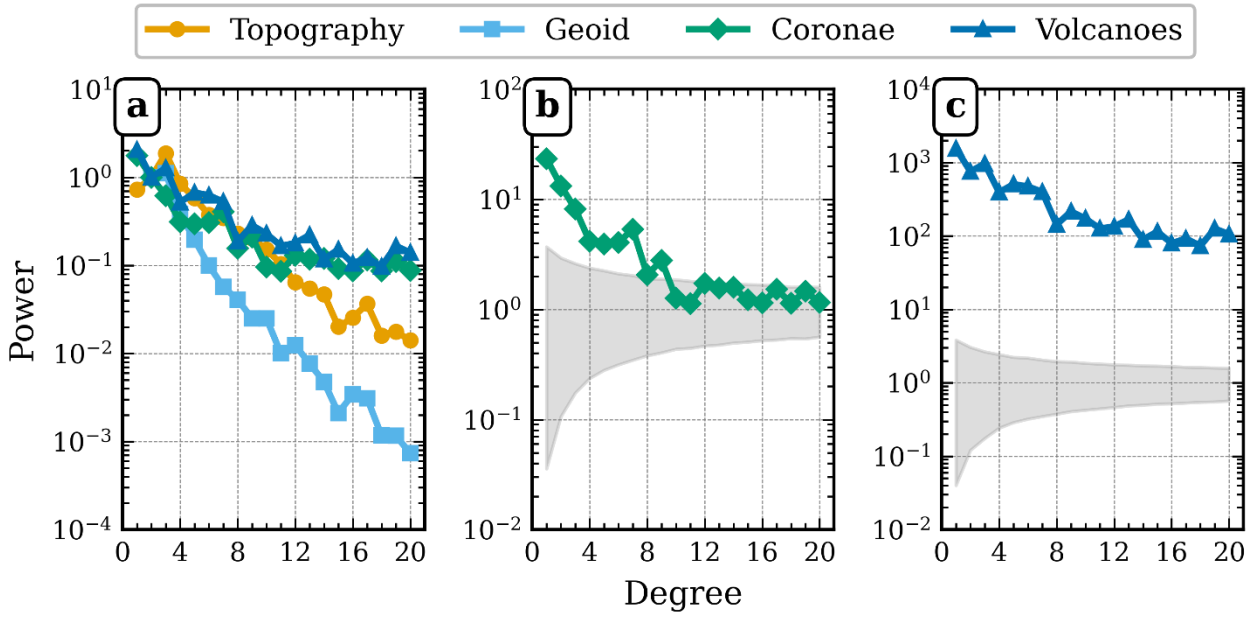

Figure 5. (a) Normalized spectral power for the full catalogue of coronae (N=545), volcanoes (N=85,021), topography, and geoid, set to equal 1 at degree 2 for comparison. Spectra for coronae and volcanoes are white at longer wavelengths, whereas topography and geoid remain red across all wavelengths shown. Spectral power of (b) coronae and (c) volcanoes without

normalizing to degree 2. The grey areas in panels (b) and (c) represent the 1st to 99th percentile bounds for 10,000 randomly generated samples of coronae and volcanoes, respectively.

Figure 6a shows the normalized spectra for all volcanoes, volcanoes ≤ 63 km, volcanoes > 63 km, and volcanic fields, which contain high concentrations of shield volcanoes with diameters ≤ 20 km as described by Hahn & Byrne (2023). The population of volcanoes is dominated by edifices ≤ 63 km in diameter. Thus, these data have indistinguishable differences in the shape of their spectra, and are perfectly positively correlated. As a result, observations regarding spectra and correlations involving volcanoes ≤ 63 km diameter are valid for the spectrum of the full catalogue. The volcanic fields spectrum shares a similar shape to the full catalogue, but with less power loss at shorter wavelengths.

For volcanoes larger than 63 km in diameter, the spectral pattern diverges at spherical harmonic degrees greater than 12, becoming relatively blue (power increasing with wavelength). Given that the minimum diameter of coronae is approximately 60 km, our analysis focuses on comparing coronae with volcanoes larger than 63 km in diameter. The spectral shapes of these two datasets exhibit near-identical features at $l \leq 4$.

In terms of formal correlation, coronae show strong alignment with all subsets of volcanoes at $l = 4$. However, the correlation between coronae and volcanoes > 63 km weakens as the harmonic degree increases, though it remains above the 80% confidence interval around $l = 8$ and $l = 14$. The minimum diameter of coronae is approximately 60 km. For this reason, we focus our comparison of corona and volcanoes with those that are > 63 km in diameter. The similarities in the shape of their spectrum are nearly identical when $l \leq 4$ (Figure 6a). Coronae are strongly correlated with volcanoes and volcano subsets at $l = 4$. Correlations between volcanoes > 63 km and coronae weakens with harmonic degree, but is above the 80% confidence interval around $l = 8$ and $l = 14$ (Figure 6b).

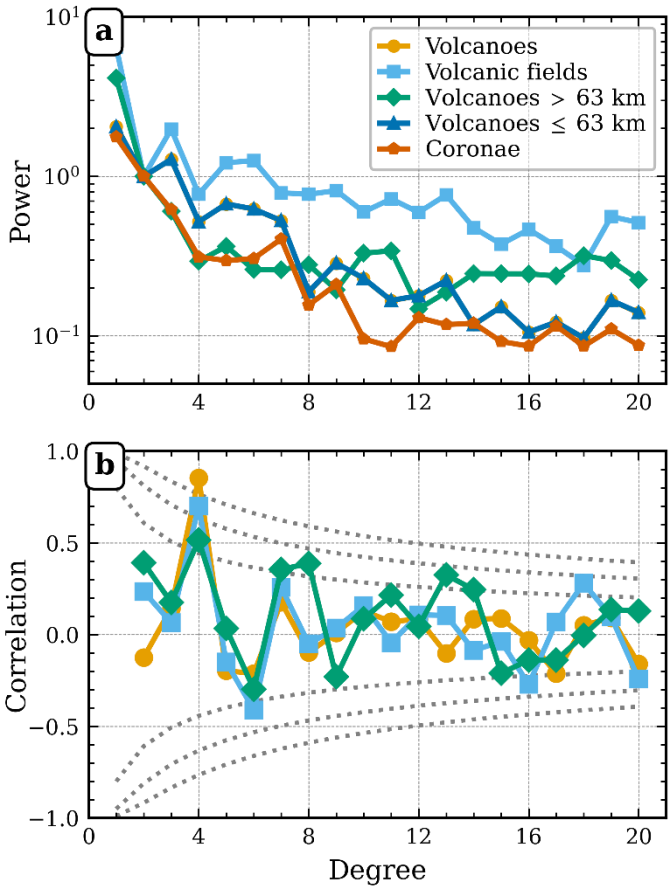

Figure 6. (a) Normalized spectra for coronae and the full catalogue and subsets of volcanoes, set to equal 1 at l =2 for comparison. The spectral pattern for the full population of volcanoes closely resembles that of volcanoes ≤ 63 km (N=84,894), which accounts for more than 99% of the total population. (b) Correlation between coronae and volcanoes, volcanic fields, and volcanoes > 63 km. Dotted lines represent 80%, 95% and 99% confidence intervals, indicating a 20%, 5%, and 1% chance of randomness in correlation coefficients for points outside these lines, respectively. The colors in (b) correspond to those in (a).

4 Discussion

Venus provides a unique context for investigating the relationship between mantle dynamics, surface topography, and volcanic activity. On Earth, the main source of mantle circulation is the cooling and sinking of oceanic lithosphere. While mantle plumes have a somewhat auxiliary role in Earth's heat budget, they are nonetheless driven by large-scale convection in the mantle (e.g., Davies & Richards, 1992; Lay et al., 2008; Sleep, 1990). In contrast, Venus may have two modes of mantle plumes: continuous axisymmetric mantle upwellings and transient thermals (Johnson & Richards, 2003; Robin et al., 2007). The

interaction of the latter with the lithosphere produces the surface expression of a corona, although the precise mechanism remains a matter of debate (e.g., Dombard et al., 2007; Gülcher et al., 2020; Smrekar and Stofan, 1997; Tucker & Dombard, 2023a). The spectral analysis of the spatial distribution of coronae and volcanic features provides valuable insights into these complex geodynamic processes. The results have significant implications for our understanding of corona formation, the role of volcanic activity, and the broader mantle dynamics on Venus.

The lack of correlation between coronae and both topography and gravity on Venus (Figure 7) is likely attributable to the coupled nature of large-scale mantle convection and transient thermal plumes. Johnson and Richards (2003) proposed that the relative absence of coronae in the lowland regions is due to the suppression of transient thermals by broad downwelling of cold lithosphere underlying these regions. Further, the concentration of coronae in the BAT region, while also being absent from the direct vicinity of active volcanic highlands in the BAT region, can be explained by the "capture" of transient thermals by the broad upwellings in the region. The correlation between topography and large volcanoes supports this hypothesis (Figure 7), as the long-wavelength topography and gravity of Venus are associated with large-scale upwelling (e.g., Anderson & Smrekar, 2006; Grimm & Phillips; 1992; Kiefer & Hager, 1992; Smrekar, 1994; Smrekar & Phillips, 1991).

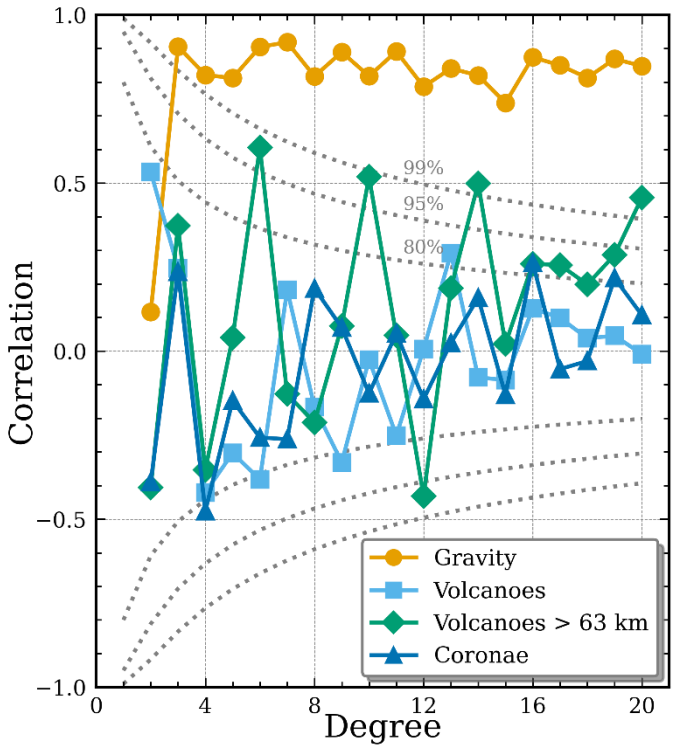

Figure 7. Correlation between topography and gravity, volcanoes, volcanoes > 63 km, and coronae. Dotted lines represent 80%, 95% and 99% confidence intervals, indicating a 20%, 5%, and 1% chance of randomness in correlation coefficients for points outside these lines, respectively.

Aphrodite and Ishtar Terrae are dominant in degrees up to 4 topography (Figure 8). The scarcity of volcanoes and coronae within these highlands contributes to the lack of correlation between topography and volcanic features at this spherical harmonic degree. Further, these regions explain the significant difference between the spectral power of volcanoes and the bounds of the random samples (Figure 5c). The random sampling was not limited by geologic boundaries; however, by constraining the latitude range for random sampling from the start to sizes comparable to Aphrodite and Ishtar (a computationally inexpensive way to prevent sampling from regions), the spectral power increases to a magnitude similar to that for the volcano dataset (Supporting Information Figure S1).

The dearth of volcanic features observed in these highland plateaus can be ascribed to crustal thickening (e.g., James et al., 2013). These compensated highlands may represent old, thickened crust making it difficult for plumes to penetrate in these regions (Johnson & Richards, 2003). Conversely, the strong correlation between volcanic features at $l = 4$ (Figure 6) is caused by the BAT region clustering (Figure 8b).

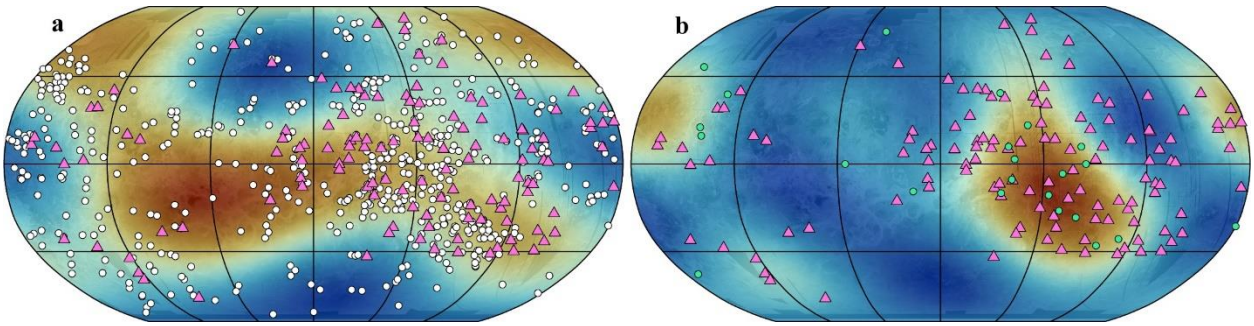

Figure 8. Robinson projected maps, centered at 180°E, of (a) degree 4 truncated spherical harmonic expansion of topography where low elevation is represented by blue and red it high elevation, and (b) degree 4 truncated representation of the spherical harmonic expansion of the full coronae dataset were blue represents low density and red represents high density regions. Both maps are underlain by Magellan SAR mosaic. Pink triangles are locations of volcanoes >63 km in diameter, white circles (a) are corona locations, and green circles (b) are coronae with

divergent lava flows. The highland plateaus of Aphrodite Terra (60°E-150°E, ~30°S) and Ishtar Terra (300°E to 60°E, ~75°N) are both largely represented in (a), the degree 4 topography, but are absent from (b), the degree 4 representation of coronae.

The spectral analysis of divergent coronae reveals characteristics that align closely with those of the full population, supporting our assertion that they represent a subset of the population rather than a distinct group. The concentration of divergent coronae in the BAT region, consistent with the distribution of the full corona population, further supports this conclusion. The post-emplacement change in slope direction of lava flows suggests a potential shift or migration of the magmatic source (Tucker & Dombard, 2023a). Changes in stress orientations could allow for new pathways for magma accent, facilitating migration away from the interior and towards the fracture annulus (e.g., McGovern et al., 2013). The spatial relationship of these divergent coronae to the complete catalogue, especially their concentration in the BAT region, implies that this mechanism is integral to their formation rather than being a consequence of some other regional or random phenomenon. The “white” spectrum and lack of correlation seen in nondivergent coronae (Figure 8) is likely due to the small sample size. However, the limited number of observed nondivergent coronae reinforces our interpretation that this process is an intrinsic part of corona formation.

The relationship between volcanism and coronae is well established (e.g., Head et al., 1992; Roberts & Head, 1993). With few exceptions, the magmatic relationship is rarely explicitly incorporated in geophysical models of formation (e.g., Dombard et al., 2007; Lang & López, 2015), instead focusing on the dynamics of the plume-lithosphere interaction. In addition to observations of volcanism at coronae, the long wavelength spectral similarities between coronae and volcanoes > 63 km suggest that they are influenced by the same long-wavelength mantle dynamics.

In addition to the direct observations of volcanic activity at coronae, the spectral analysis reveals similarities between coronae and large volcanoes. Specifically, the long-wavelength spectral characteristics of these features exhibit similar trends as well as correlation (> 80% confidence) at various long-wavelength scales. This correlation is further strengthened by the observed clustering of coronae and large volcanoes in the BAT region. The patterns observed align well with models that invoke mantle material upwelling and its interaction with the

lithosphere, resulting in volcanic activity and surface deformation. The strong correlation at low spherical harmonic degrees and shared spatial distribution underline a likely commonality in the mantle processes that drive coronae formation.

5 Conclusion

Observations of coronae from SAR images show many associated volcanic features and landforms. By mapping discrete lava flows within corona fracture annuli, we have developed a new subset of the corona dataset of coronae with topography that has changed since the emplacement of those lava flows. Spectral power analysis of the distribution of divergent coronae shows that they are a part of the same distribution of the full population of coronae, rather than a random or regional occurrence. Furthermore, coronae have a strong correlation and spectral shape at low spherical harmonic degrees with volcanoes of comparable scale suggesting a shared geodynamic origin.

These observations underscore the significance of volcanism and highlight the need for future investigations that incorporate magmatic processes into models of corona formation, instead of models that ascribe coronae as the products of plume/lithosphere interactions. As with many studies that rely on surface observations of Venus, improved resolution of surface SAR imagery, topography, and gravity data would further refine our understanding of the geologic and geophysical processes related to coronae and volcanism. Improved data would likely increase the number of coronae at which divergent lava flows due to better identification of flow margins. Additionally, it would allow for measurements of flow divergence to be better constrained.

Acknowledgments

Portions of this work were funded by the Illinois Space Grant Consortium. Early portions of this work were presented at the Lunar and Planetary Science Conference with support from the University of Illinois Chicago LAS Travel Award.

Open Research

The global catalog of volcanoes developed by Hahn and Byrne (2023) is available through the Washington University in St. Louis Open Scholarship repository (Hahn & Byrne,

2022). The Stofan et al. (2001a) catalogue of Type 1 and Type 2 coronae is available through the NASA Planetary Data System (Stofan et al., 2001b). NASA Magellan Mission data, including full-resolution and compressed SAR images (Pettengill, 1991) and global topography data (Ford, 1992), and stereo-derived topography data (Herrick, 2020) is available from the NASA Planetary Data System. A portion of the spherical harmonic calculations were performed using SHTools (Wieczorek & Meschede, 2018). The Venus topography model, VenusTopo719 (Wieczorek, 2015), and gravity model, MGNP180U (Konopliv et al., 1999), are available through the *datasets* submodule in SHTools. The Python code SHPointPower for the spherical harmonic analysis is available via GitHub (Tucker, 2023), and GIS shapefiles of the mapped lava flow centerlines are available via Zenodo (Tucker & Dombard, 2023b).

References

Anderson, F. S., & Smrekar, S. E. (2006). Global mapping of crustal and lithospheric thickness on Venus. *Journal of Geophysical Research*, *111*(8), 1–20. https://doi.org/10.1029/2004JE002395

Arvidson, R. E., Greeley, R., Malin, M. C., Saunders, R. S., Izenberg, N., Plaut, J. J., et al. (1992). Surface modification of Venus as inferred from Magellan observations of plains. *Journal of Geophysical Research*, *97*(E8), 13303. https://doi.org/10.1029/92JE01384

Aubele, J. C., & Slyuta, E. N. (1990). Small domes on Venus: Characteristics and origin. *Earth, Moon and Planets*, *50–51*(1), 493–532. https://doi.org/10.1007/BF00142404

Barsukov, V. L., Basilevsky, A. T., Burba, G. A., Bobinna, N. N., Kryuchkov, V. P., Kuzmin, R. O., et al. (1986). The geology and geomorphology of the Venus surface as revealed by the radar images obtained by Veneras 15 and 16. *Journal of Geophysical Research*, *91*(B4), 378–398. https://doi.org/10.1029/JB091iB04p0D378

Bindschadler, D. L., Schubert, G., & Kaula, W. M. (1992). Coldspots and hotspots: Global tectonics and mantle dynamics of Venus. *Journal of Geophysical Research*, *97*(E8), 13495. https://doi.org/10.1029/92JE01165

Copp, D. L., Guest, J. E., & Stofan, E. R. (1998). New insights into Coronae evolution: Mapping on Venus. *Journal of Geophysical Research*, *103*(E8), 19401–19417. https://doi.org/10.1029/97JE03182

Davaille, A., Smrekar, S. E., & Tomlinson, S. (2017). Experimental and observational evidence for plume-induced subduction on Venus. *Nature Geoscience*, *10*(5), 349–355. https://doi.org/10.1038/ngeo2928

Davies, G. F., & Richards, M. A. (1992). Mantle Convection. *The Journal of Geology*, *100*(2). https://doi.org/https://doi.org/10.1086/629582

DeLaughter, J. E., & Jurdy, D. M. (1999). Corona Classification by Evolutionary Stage. *Icarus*, *139*(1), 81–92. https://doi.org/10.1006/icar.1999.6087

Dombard, A. J., Johnson, C. L., Richards, M. A., & Solomon, S. C. (2007). A magmatic loading model for coronae on Venus. *Journal of Geophysical Research*, *112*(4), 1–13. https://doi.org/10.1029/2006JE00273

Ford, P. G. (1992). MGN V RDRS 5 global data record topographic V1.0 [Dataset]. NASA Planetary Data System. https://doi.org/10.17189/1522522

Gerya, T. V. (2014). Plume-induced crustal convection: 3D thermomechanical model and implications for the origin of novae and coronae on Venus. *Earth and Planetary Science Letters*, *391*, 183–192. https://doi.org/10.1016/j.epsl.2014.02.005

Glaze, L. S., Stofan, E. R., Smrekar, S. E., & Baloga, S. M. (2002). Insights into corona formation through statistical analyses. *Journal of Geophysical Research*, *107*(E12), 18-1-18–12. https://doi.org/10.1029/2002JE001904

Grimm, R. E., & Phillips, R. J. (1992). Anatomy of a Venusian hot spot: Geology, gravity, and mantle dynamics of Eistla Regio. *Journal of Geophysical Research*, *97*(E10), 16035. https://doi.org/10.1029/92JE01500

Guest, J. E., Bulmer, M. H., Aubele, J. C., Beratan, K. K., Greeley, R., Head, J. W., et al. (1992). Small volcanic edifices and volcanism in the plains of Venus. *Journal of Geophysical Research: Planets*, *97*(E10), 15949–15966. https://doi.org/10.1029/92JE01438

Guest, J. E., & Stofan, E. R. (1999). A New View of the Stratigraphic History of Venus. *Icarus*, *139*(1), 55–66. https://doi.org/10.1006/icar.1999.6091

Gülcher, A. J. P., Gerya, T. V., Montési, L. G. J., & Munch, J. (2020). Corona structures driven by plume–lithosphere interactions and evidence for ongoing plume activity on Venus. *Nature Geoscience*, *13*(8), 547–554. https://doi.org/10.1038/s41561-020-0606-1

Hahn, R. M., & Byrne, P. K. (2022). A global catalog of volcanoes and volcanic fields on Venus [V2] (version 2) [Dataset]. Washington University in St. Louis. https://doi.org/10.7936/8XY0-X885

Hahn, R. M., & Byrne, P. K. (2023). A Morphological and Spatial Analysis of Volcanoes on Venus. *Journal of Geophysical Research: Planets*, *128*(4), 1–26. https://doi.org/10.1029/2023JE007753

Hansen, V. L. (2002). Artemis: Surface expression of a deep mantle plume on Venus. *Bulletin of the Geological Society of America*, *114*(7), 839–848. https://doi.org/10.1130/0016-7606(2002)114<0839:ASEOAD>2.0.CO;2

Hauck, S. A. I., Phillips, R. J., & Price, M. H. (1998). Venus: Crater distribution and plains resurfacing models. *Journal of Geophysical Research: Planets*, *103*(E6), 13635–13642. https://doi.org/10.1029/98JE00400

Head, J. W., Crumpler, L. S., Aubele, J. C., Guest, J. E., & Saunders, R. S. (1992). Venus volcanism: Classification of volcanic features and structures, associations, and global distribution from Magellan data. *Journal of Geophysical Research*, *97*(E8), 13153. https://doi.org/10.1029/92JE01273

Herrick, R. R. (2020). Magellan Venus stereo-derived topography Bundle. [Dataset]. Geosciences Node. https://doi.org/https://doi.org/10.17189/1519332

Herrick, R. R., & Hensley, S. (2023). Direct Observation of Volcanic Activity on Venus from Repeat Magellan Imaging. In L. and P. Institute (Ed.), *54th Lunar and Planetary Science Conference*. Retrieved from https://www.hou.usra.edu/meetings/lpsc2023/pdf/1061.pdf

Herrick, R. R., & Sharpton, V. L. (2000). Implications from stereo-derived topography of Venusian impact craters. *Journal of Geophysical Research: Planets*, *105*(E8), 20245–20262. https://doi.org/10.1029/1999JE001225

Herrick, R. R., Sharpton, V. L., Malin, M. C., Lyons, S. N., & Feely, K. (1997). Morphology and Morphometry of Impact Craters. In S. W. Bougher, D. M. Hunten, R. J. Phillips (Eds.), *Venus II: Geology, Geophysics, Atmosphere, and Solar Wind Environment* (pp. 1015–1046). Tucson, AZ: The University of Arizona Press.

Herrick, R. R., Stahlke, D. L., & Sharpton, V. L. (2012). Fine-scale Venusian topography from Magellan stereo data. *Eos, Transactions American Geophysical Union*, *93*(12), 125–126. https://doi.org/10.1029/2012EO120002

Hoogenboom, T., & Houseman, G. A. (2006). Rayleigh-Taylor instability as a mechanism for corona formation on Venus. *Icarus*, *180*(2), 292–307. https://doi.org/10.1016/j.icarus.2005.11.001

Ivanov, M. A., Crumpler, L. S., Aubele, J. C., & Head, J. W. (2015). Volcanism on Venus. In H. Sigurdsson (Ed.), *The Encyclopedia of Volcanoes* (Second Edi, pp. 729–746). Academic Press. https://doi.org/10.1016/B978-0-12-385938-9.00042-0

James, P. B., Zuber, M. T., & Phillips, R. J. (2013). Crustal thickness and support of topography on Venus. *Journal of Geophysical Research: Planets*, *118*(4), 859–875. https://doi.org/10.1029/2012JE004237

Janes, D. M., & Squyres, S. W. (1995). Viscoelastic relaxation of topographic highs on Venus to produce coronae. *Journal of Geophysical Research*, *100*(E10), 21173. https://doi.org/10.1029/95je01748

Jellinek, A. M., Lenardic, A., & Manga, M. (2002). The influence of interior mantle temperature on the structure of plumes: Heads for Venus, Tails for the Earth. *Geophysical Research Letters*, *29*(11), 1532. https://doi.org/10.1029/2001GL014624

Johnson, C. L., & Richards, M. A. (2003). A conceptual model for the relationship between coronae and large-scale mantle dynamics on Venus. *Journal of Geophysical Research*, *108*(6), 5058. https://doi.org/10.1029/2002je001962

Kiefer, W. S., & Hager, B. H. (1992). Geoid anomalies and dynamic topography from convection in cylindrical geometry: applications to mantle plumes on Earth and Venus. *Geophysical Journal International*, *108*(1), 198–214. https://doi.org/10.1111/j.1365-246X.1992.tb00850.x

Kirchoff, M. R., McKinnon, W. B., & Schenk, P. M. (2011). Global distribution of volcanic centers and mountains on Io: Control by asthenospheric heating and implications for mountain formation. *Earth and Planetary Science Letters*, *301*(1–2), 22–30. https://doi.org/10.1016/j.epsl.2010.11.018

Koch, D. M., & Manga, M. (1996). Neutrally buoyant diapirs: A model for Venus coronae. *Geophysical Research Letters*, *23*(3), 225–228. https://doi.org/10.1029/95GL03776

Konopliv, A. S., Banerdt, W. B., & Sjogren, W. L. (1999). Venus Gravity: 180th Degree and Order Model. *Icarus*, *139*(1), 3–18. https://doi.org/10.1006/icar.1999.6086

Lang, N. P., & López, I. (2015). The magmatic evolution of three Venusian coronae. *Geological Society, London, Special Publications*, *401*(1), 77–95. https://doi.org/10.1144/SP401.3

Lay, T., Hernlund, J., & Buffett, B. A. (2008). Core–mantle boundary heat flow. *Nature Geoscience*, *1*(1), 25–32. https://doi.org/10.1038/ngeo.2007.44

McGovern, P. J., Rumpf, M. E., & Zimbelman, J. R. (2013). The influence of lithospheric flexure on magma ascent at large volcanoes on Venus. *Journal of Geophysical Research: Planets*, *118*(11), 2423–2437. https://doi.org/10.1002/2013JE004455

McKenzie, D., Ford, P. G., Johnson, C. L., Parsons, B., Sandwell, D. T., Saunders, R. S., & Solomon, S. C. (1992). Features on Venus generated by plate boundary processes. *Journal of Geophysical Research*, *97*(E8), 13533. https://doi.org/10.1029/92JE01350

McKinnon, W. B., Zahnle, K. B., Ivanov, B. A., & Melosh, H. J. (1997). Cratering on Venus. In S. W. Bougher, D. M. Hunten, & R. J. Phillips (Eds.), *Venus II: Geology, Geophysics, Atmosphere, and Solar Wind Environment* (pp. 969–1014). Tucson, AZ: The University of Arizona Press.

Pettengill, G. (1991) MGN V RDRS derived mosaic image data record full res (V1.0 [Dataset]. NASA Planetary Data System. https://doi.org/10.17189/1522523

Phillips, R. J., & Malin, M. C. (1983). The interior of Venus and tectonic implications. In D. M. Hunten, L. Colin, T. M. Donahue, & V. I. Moroz (Eds.), *Venus* (pp. 159–214). Tucson, AZ: The University of Arizona Press. https://doi.org/https://doi.org/10.2307/j.ctv25c4z16.

Phillips, R. J., Raubertas, R. F., Arvidson, R. E., Sarkar, I. C., Herrick, R. R., Izenberg, N., & Grimm, R. E. (1992). Impact Craters and Venus Resurfacing History. *Journal of Geophysical Research*, *97*(E10), 15923. https://doi.org/10.1029/92JE01696

Rappaport, N. J., Konopliv, A. S., Kucinskas, A. B., & Ford, P. G. (1999). An Improved 360 Degree and Order Model of Venus Topography. *Icarus*, *139*(1), 19–31. https://doi.org/10.1006/icar.1999.6081

Ribe, N. M., & de Valpine, D. P. (1994). The global hotspot distribution and instability of D″. *Geophysical Research Letters*, *21*(14), 1507–1510. https://doi.org/10.1029/94GL01168

Richards, M. A., Hager, B. H., & Sleep, N. H. (1988). Dynamically supported geoid highs over hotspots: observation and theory. *Journal of Geophysical Research*, *93*(B7), 7690–7708. https://doi.org/10.1029/JB093iB07p07690

Roberts, K. M., & Head, J. W. (1993). Large-scale volcanism associated with coronae on Venus: Implications for formation and evolution. *Geophysical Research Letters*, *20*(12), 1111–1114. https://doi.org/10.1029/93GL01484

Robin, C. M. I., Jellinek, A. M., Thayalan, V., & Lenardic, A. (2007). Transient mantle convection on Venus: The paradoxical coexistence of highlands and coronae in the BAT

region. *Earth and Planetary Science Letters*, *256*(1–2), 100–119. https://doi.org/10.1016/j.epsl.2007.01.016

Russell, M. B., & Johnson, C. L. (2021). Evidence for a Locally Thinned Lithosphere Associated with Recent Volcanism at Aramaiti Corona, Venus. *Journal of Geophysical Research: Planets*, *126*(8), 1–19. https://doi.org/10.1029/2020JE006783

Sandwell, D. T., & Schubert, G. (1992). Evidence for Retrograde Lithospheric Subduction on Venus. *Science*, *257*(5071), 766–770. https://doi.org/10.1126/science.257.5071.766

Schaber, G. G., Strom, R. G., Moore, H. J., Soderblom, L. A., Kirk, R. L., Chadwick, J., et al. (1992). Geology and distribution of impact craters on Venus: What are they telling us? *Journal of Geophysical Research*, *97*(E8), 13257. https://doi.org/10.1029/92JE01246

Silverman, B. W. (1998). *Density Estimation for Statistics and Data Analysis.* Routledge. https://doi.org/10.2307/2347507

Sleep, N. H. (1990). Hotspots and mantle plumes: Some phenomenology. *Journal of Geophysical Research*, *95*(B5), 6715. https://doi.org/10.1029/JB095iB05p06715

Slyuta, E. N. (1990). Large Shield Volcanoes (>100 Km in Diameter) on Venus: Morphologic Types. In *21st Lunar and Planetary Science Conference*. Retrieved from https://articles.adsabs.harvard.edu/full/1990LPI....21.1172S

Slyuta, E. N., & Kreslavsky, M. A. (1990). Intermediate (20-100 Km) Sized Volcanic Edifices on Venus. In *21st Lunar and Planetary Science Conference*. Retrieved from https://articles.adsabs.harvard.edu/full/1990LPI....21.1174S

Smrekar, S. E. (1994). Evidence for Active Hotspots on Venus from Analysis of Magellan Gravity Data. *Icarus*, *112*(1), 2–26. https://doi.org/10.1006/icar.1994.1166

Smrekar, S. E., Davaille, A., & Sotin, C. (2018). *Venus Interior Structure and Dynamics*. *Space Science Reviews* (Vol. 214). Springer Nature B.V. https://doi.org/10.1007/s11214-018-0518-1

Smrekar, S. E., Kiefer, W. S., & Stofan, E. R. (1997). Large volcanic rises on Venus. In S. W. Bougher, D. M. Hunten, & R. J. Phillips (Eds.), *Venus II: Geology, Geophysics, Atmosphere, and Solar Wind Environment* (pp. 845–878). Tucson, AZ: University of Arizona Press.

Smrekar, S. E., & Phillips, R. J. (1991). Venusian highlands: geoid to topography ratios and their implications. *Earth and Planetary Science Letters*, *107*(3–4), 582–597. https://doi.org/10.1016/0012-821X(91)90103-O

Smrekar, S. E., & Stofan, E. R. (1999). Origin of Corona-Dominated Topographic Rises on Venus. *Icarus*, *139*(1), 100–115. https://doi.org/10.1006/icar.1999.6090

Smrekar, S. E., Stofan, E. R., Mueller, N., Treiman, A. H., Elkins-Tanton, L. T., Helbert, J., et al. (2010). Recent hotspot volcanism on Venus from VIRTIS emissivity data. *Science*, *328*(5978), 605–608. https://doi.org/10.1126/science.1186785

Squyres, S. W., Janes, D. M., Baer, G., Bindschadler, D. L., Schubert, G., Sharpton, V. L., & Stofan, E. R. (1992). The morphology and evolution of coronae on Venus. *Journal of Geophysical Research*, *97*(E8), 13611. https://doi.org/10.1029/92je01213

Squyres, S. W., Janes, D. M., Schubert, G., Bindschadler, D. L., Moersch, J. E., Turcotte, D. L., & Stofan, E. R. (1993). The spatial distribution of coronae and related features on Venus. *Geophysical Research Letters*, *20*(24), 2965–2968. https://doi.org/10.1029/93GL00866

Stofan, E. R., Hamilton, V. E., Janes, D. M., & Smrekar, S. E. (1997). Coronae on Venus: Morphology and Origin. In S. W. Bougher, D. M. Hunten, & R. J. Phillips (Eds.), *Venus II: Geology, Geophysics, Atmosphere, and Solar Wind Environment* (pp. 931–965). Tucson, AZ: University of Arizona Press. https://doi.org/10.2307/j.ctv27tct5m

Stofan, E. R., Sharpton, V. L., Schubert, G., Baer, G., Bindschadler, D. L., Janes, D. M., & Squyres, S. W. (1992). Global distribution and characteristics of coronae and related features on Venus: Implications for origin and relation to mantle processes. *Journal of Geophysical Research*, *97*(E8), 13347. https://doi.org/10.1029/92JE01314

Stofan, E. R., Smrekar, S. E., Bindschadler, D. L., & Senske, D. A. (1995). Large topographic rises on Venus: Implications for mantle upwelling. *Journal of Geophysical Research*, *100*(E11), 23317. https://doi.org/10.1029/95JE01834

Stofan, E. R., Smrekar, S. E., Tapper, S. W., Guest, J. E., & Grindrod, P. M. (2001a). Preliminary analysis of an expanded corona database for Venus. *Geophysical Research Letters*, *28*(22), 4267–4270. https://doi.org/10.1029/2001GL013307

Stofan, E. R., Smrekar, S. E., Tapper, S. W., Guest, J. E., & Grindrod, P. M. (2001b). Preliminary analysis of an expanded corona database for Venus. NASA Planetary Data System. https://pdsimage2.wr.usgs.gov/pub/pigpen/venus/Coronae/

Strom, R. G., Schaber, G. G., & Dawson, D. D. (1994). The global resurfacing of Venus. *Journal of Geophysical Research*, *99*(E5), 10,899-10,926. https://doi.org/10.1029/94JE00388

Tucker, W. S. (2023). *SHPointPower* (v1.0.0) [Software]. Zenodo. https://doi.org/10.5281/zenodo.10084438

Tucker, W. S. & Dombard, A. J. (2023a). Evidence of Topographic Change Recorded by Lava Flows at Atete and Aruru Coronae on Venus. *Journal of Geophysical Research: Planets*, 128, e2023JE007971. https://doi.org/10.1029/2023JE007971

Tucker, W. S. & Dombard, A. J. (2023b) SI files for Spherical-harmonic distribution of coronae in relation to volcanic features on Venus. [Dataset]. Zenodo. https://doi.org/10.5281/zenodo.10144166

Wieczorek, M. A. (2015). Gravity and topography of the terrestrial planets. In G. Schubert & T. Spohn (Eds.), *Treatise on Geophysics* (2nd ed., Vol. 10, pp. 153–193). Oxford, UK: Elsevier-Pergamon. https://doi.org/10.1016/B978-0-444-53802-4.00169-X

Wieczorek, M. A., & Meschede, M. (2018). SHTools: Tools for Working with Spherical Harmonics. *Geochemistry, Geophysics, Geosystems*, *19*(8), 2574–2592. https://doi.org/10.1029/2018GC007529